Geosci. Instrum. Method. Data Syst. Discuss., 4, 165–190, 2014
www.geosci-instrum-method-data-syst-discuss.net/4/165/2014/
doi:10.5194/gid-4-165-2014

Geoscientific Instrumentation Methods and Data Systems Discussions
Open Access

A new mobile and portable scanning lidar for profiling lower troposphere

C.-W. Chiang[1,3], S. K. Das[2,3], H.-W. Chiang[1], J.-B. Nee[3], S.-H. Sun[1], S.-W. Chen[4], P.-H. Lin[4], J.-C. Chu[4], C.-S. Su[4], and L.-S. Su[5]

[1]Department of Mechanical Engineering, Kun Shan University, Tainan, Taiwan
[2]Indian Institute of Tropical Meteorology, Pune, India
[3]Department of Physics, National Central University, Chungli, Taiwan
[4]Taoyuan County Government Environment Protection Bureau, Taoyuan, Taiwan
[5]EI-LIDAR Corporation Limited, Taichung, Taiwan

Received: 20 February 2014 – Accepted: 23 March 2014 – Published: 9 April 2014

Correspondence to: C.-W. Chiang (cwchiang@alumni.ncu.edu.tw)

Published by Copernicus Publications on behalf of the European Geosciences Union.

Abstract

We present and discuss on an indigenously developed mobile and portable 3-D scanning lidar system. The system utilizes a stimulated Raman-scattering technique for the continuous observation of atmospheric aerosols, clouds and trace gases. The system provides fast scanning technique with a high speed data acquisition, which permits the real-time measurement of air pollutant mobility. The temporal resolution of data retrieval is every one min. The scanning lidar system provides typical horizontal coverage of about 8–10 km when scanning, while the vertical range can be up to 20 km depending upon the laser power and sky conditions. This versatile lidar system has also overcome the drawbacks which are popular in the other scanning lidar system such as complicated operation; overlapping height between laser beam and telescope field of view; and damage of optic detectors for long duration measurement by using an integral coaxial transmitter and receiver. Some of the initial results obtained from the scanning lidar system are also presented. We have shown that the developed 3-D scanning lidar system can resolve the boundary layer structure and land-sea breeze circulation. Discussion is also made on the application of scanning lidar system to measure pollutant over industrial areas.

1 Introduction

Aerosols, clouds, and trace gases are among the principal atmospheric variables which alters the radiative balance of the earth-atmosphere system. Therefore, over the last several decades, the atmospheric scientists have shown great interest to characterize aerosol, cloud and trace gases to understand their impact on climate change and weather system (Bach, 1976; Twomey, 1991; Kaufman et al., 2002; Mattis et al., 2004). The remote sensing technique is used to have profile measurement of atmospheric variables such as aerosol, cloud and trace gases. The optical remote sensing instruments like light detection and ranging (lidar), which is based on the principle of laser

GID
4, 165–190, 2014

spectroscopy has been proven to have a great potential to probe the earth's atmosphere due to their sensitivity, selectivity and range resolved data of meteorological variables and atmospheric constituents (Fredriksson et al., 1981; Muruyama et al., 2001; Ansmann et al., 2003). The lidar system provides real-time monitoring of various atmospheric variables (such as aerosol, cloud, temperature, water vapor, optical depth of particulate matter, etc.) and meteorological processes (boundary layer growth, aerosol and cloud layering, etc.).

In the last 15 years, we have set up indigenously developed lidar system at the National Central University (NCU), Chung-Li (25° N, 121° E), Taiwan to understand the vertical distribution of aerosol (Chiang et al., 2004, 2007, 2008a, 2008b, 2012), cloud (Nee et al., 1998; Chen et al., 2002; Das et al., 2009) and other meteorological variables such as temperature (Nee et al., 1995; Chen et al., 2004) and water vapour (Chiang et al., 2009). The NCU lidar system is fixed at the ground and can be operated in the nighttime only, which limit the investigation of spatial distribution and the diurnal cycle (associated with orography and atmospheric conditions) of the atmospheric variables.

To understand the variability of aerosol, cloud, and trace gases on different scales, both spatially and temporally, the lidar techniques are now advancing a state of art with the development of powerful computer-controlled instruments. In view of the importance of aerosol and cloud measurement, the 3-D scanning lidar is most appropriate and foremost to do routine observation automatically (Mayor and Spuler, 2004; Radlach et al., 2008; Behrendt et al., 2009, 2011). In this context, we have indigenously developed mobile and portable 3-D scanning lidar system to investigate the aerosol and trace gas properties in the lower troposphere, which is capable of day and night time operation. Therefore, the limiting factor for continuous data collection is bad weather or logistic problem. The scanning measurement technique will help to understand the chemical and physical processes of the atmospheric pollutants caused by the planetary boundary layer (PBL) dynamics/evolution, where the conventional point-sampling instruments are insufficient. Our 3-D scanning lidar is mobile and portable and have many added advantage over the conventional lidar system.

The aim of this paper is to report the design of a newly developed 3-D scanning lidar. The operating features and data analysis techniques are also discussed. Some of the preliminary results and the potential application of the scanning lidar are also presented. The paper is presented as follows: the system description and capabilities are discussed in Sect. 2. The methodology and analysis technique are described in Sect. 3. Some of the initial results of the measurement are presented in Sect. 4. Finally, a summary in Sect. 5 will concludes the paper.

2 System description and capabilities

Figure 1a shows the photographic image and the prototype model (shown in Fig. 1b) of the scanning lidar. The system includes the laser as a transmitter, Schmidt–Cassegrain telescope as a receiver, photomultiplier tube as a detector and real-time data acquisition and signal processing unit. The laser, telescope and scanner are mounted on a vibration-isolated platform (to protect the laser and optical instrument against bumps in mobile application) in an aluminum framework to have a good structural stability. The power supply required for the operation of lidar is meet either from commercial mains or Honda diesel power generator (rating 220 VAC ± 10 %, 50 Hz ± 10 %). Technical specifications of the lidar system are given in Table 1.

A Nd:YAG (Neodymium : yttrium-Aluminum-Garnet) pulsed solid state laser is used as a laser source. The laser pulse width is ∼ 10 ns and repetition rate is 10 Hz. The laser operation is based on the second, third and fourth harmonic frequency generation at 532, 355 and 256 nm respectively. The transmitted energy is about 500, 330, 200 and 90 mJ at 1064, 532, 355 and 266 nm respectively. The divergence of the laser beam is about 0.5 mrad. The laser is mounted on an optical bench having the facility of height adjustment. Seven reflection mirror (shown as 1 to 7 in Fig. 1b), which is a thick hard coated flat type, are mounted at 45° with respect to the lidar system surface to direct the laser beam into the atmosphere. The mirrors have the provision of precise adjustment of azimuth and tilting of the laser beam. In case of breakdown of the laser transmitter, a safety interlock is provided to shut down the laser unit.

The atmospheric species are sensitive to different wavelengths. Therefore, multi-wavelength laser must be in practice for the measurement of different atmospheric species. To achieve multi-wavelength, the Nd: laser is allowed to pass through various Raman active gas enclosed in a cell. The cell is known as Raman cell and the method is known as Raman cell technique. We have indigenously designed and developed a Raman cell (single pass) of 1.5 m long and 2 cm diameter. Two lenses (L1 and L2) are used in the Raman cell. L1 is used at the head of the Raman cell to control the confocal parameter of the pump laser beam. L2 is configured at the end of the cell to collimate the output beam from the Raman cell. The focal length of the input and output cell lenses is about 75 cm. Two similar configurations of Raman cells are used. One cell is filled with H_2 at 5 atm and pumped with fourth harmonic (266 nm) of a Nd:YAG laser generating a wavelength of about 298 nm. The partial pressure of gas in the Raman cell is variable and must be chosen for their better conversion efficiency. The second cell is filled with CH_4 at 20 atm and pumped with fourth and third harmonic (266/355 nm) of a Nd:YAG laser generating a wavelength of about 289 and 395 nm respectively. The transmitted Raman wavelength energy is about 15–30 mJ at 298, 289 and 395 nm. The fast switching of Raman cell is employed with the piezoelectric drivers. This allows the availability of multi-wavelength lidar for simultaneous measurements of several spectral overlapping atmospheric species. Therefore, the developed lidar system can be also used as a differential absorption lidar (DIAL).

A Schmidt–Cassegrain telescope (Celestron-G8) is used as the optical receiver with a focal length of f/10. The receiver telescope is capable to scan in azimuth (from 0 to 360°) and the zenith (from 0 to 180°) direction through servo motor i and ii respectively (Fig. 1b) with a minimum precision of 0.038°. At the rear end of the telescope there is a collimating lens (Fig. 1b), which focuses the entire field of view (FOV) of the telescope on to the photomultiplier tube (PMT, which is used as a detector) head. The background noise level is suppressed by using the narrow band interference filter. Behind the collimating lens, a rotating interference filter wheel (Fig. 1b) is used. The rotating wheel has 6 filters, which enables the different wavelength selection. The signals from the PMT are fed directly on to a multi-channel transient recorder (Licel TR20-160). The Licel recorder combines A/D converter (12 Bit at 20 MHz) with 250 MHz fast photon counting system in the acquisition, which allows a high dynamic range louder signal. The spatial and temporal resolution of the data acquisition in Licel recorder is 7.5 m and 1 min respectively.

In scanning lidar system to maintain the parallel optical axes between telescope and laser beam and make the alignment easier in the process of scanning is still a major concern. The coaxial mode lidar is used to maintain the parallel optical axes between telescope FOV and laser beam, which makes the alignment easier in the process of scanning. However, in most of the scanning lidar where it has coaxial mode, the backscattered light will be transmitted along the light path. This approach will generate strong background noise in the detector (i.e., PMT) and will limit the detection of backscattered signals. During continuous long run lidar operation, the coaxial mode scanning can damage the detector. Moreover, the complex procedure to guide the emitted laser beam is also inconvenient (Eichinger et al., 1999; McGill et al., 2002).

We have also designed the scanning lidar as a coaxial mode to reduce the overlapping height ($\sim$ 260 m) between transmitter and receiver. However, we have used separate path for laser transmission. The laser source is kept fixed, but the beam of laser light (path is indicated by the red line) is made to scan by using seven reflecting mirrors as shown in Fig. 1. All the reflecting mirrors used for the beam steering are numbered from 1 to 7. The laser beam can be steered in both azimuth and zenith direction by rotating the suitable reflecting mirror. This technique helps to avoid the laser transmitter being gotten damage while scanning. In earlier lidar system, the laser transmitter and telescope rotate together while scanning (Sasano, 1985). This approach can easily damage the laser transmitter, or require frequent calibration for the long-term operation.

GID
4, 165–190, 2014

All the hardware sections of the lidar system are controlled automatically via computer in the Microsoft window platform. The laser is auto-control with computer via RS232 serial port. The Licel recorder is connected to a computer via a network with TCP/IP protocol. The servo motors are connected with computer via GPIB card. The auto-controlled software of lidar has a user friendly graphical interface that makes the system operation easier.

3 Methodology and data analysis

3.1 Lidar equation

The optical power measured with a lidar is proportional to signal backscattered by the atmospheric particles and molecules. The detected lidar signal can be expressed as

$$P_\mathrm{M}(z) = P_\mathrm{L} \cdot \frac{O(z)\cdot A_\mathrm{T}}{z^2} \cdot \beta_\mathrm{atm}(z) \cdot e^{-2\int_0^z \alpha(z')\mathrm{d}z'} \tag{1}$$

where, P_M and P_L are the power received from distance z and laser output energy, respectively; $O(z)$ is the overlap function; A_T is a constant which accounts for system optical efficiency, the telescope receiver area, and the PMT spectral efficiency; $\beta_\mathrm{atm}(z)$ and $\alpha(z)$ are the backscatter and extinction coefficient of atmosphere respectively. The integral is to be taken in between heights 0 and z to derive the atmospheric transmission. The backscattering and extinction coefficients, $\beta_\mathrm{atm}(z)$ and $\alpha(z)$ are contributed both from aerosols and air molecules as shown below:

$$\beta_\mathrm{atm}(z) = \beta_\mathrm{a}(z) + \beta_\mathrm{r}(z) \tag{2}$$

$$\alpha(z) = \alpha_\mathrm{a}(z) + \alpha_\mathrm{r}(z) \tag{3}$$

where the subscripts r and a represent the air molecules and aerosols respectively.

GID
4, 165–190, 2014

3.2 DIAL technique

The Differential absorption lidar (DIAL) technique is based on the signal at two different wavelengths viz., λ_{ON} and λ_{OFF} corresponding to large and small absorption by the target species, respectively. The DIAL equation for the species concentration estimation is expressed as

$$N(z) = \frac{1}{2\Delta\sigma}\left\{\frac{d}{dz}\left[-\ln\frac{P(\lambda_{ON},z)}{P(\lambda_{OFF},z)}\right]+E_P\right\} \tag{4}$$

where, $P(\lambda_{ON},z)$ and $P(\lambda_{OFF},z)$ are the return signals from range z at λ_{ON} and λ_{OFF} respectively. $\Delta\sigma = \sigma(\lambda_{ON}) - \sigma(\lambda_{OFF})$ is the differential absorption cross section of the measured target species at temperature t; E_P is the correction term for the contribution of differential backscatter and extinction by the aerosols and molecules. Detail methodology of DIAL technique for the atmospheric trace gas measurement can be found in Gimmestad (2005 and references therein). We have used λ_{ON} and λ_{OFF} as 289 and 298 nm, respectively for the sulfur dioxide (SO_2) measurement.

3.3 Errors and uncertainties

The sources of errors and uncertainties associated with the measurements of the aerosol backscattering coefficient (β_a (z)) are the noise from the signal, uncertainty in the molecular backscattering coefficient ($\beta_r(z)$), consideration of initial value for reference distance and lidar ratio, etc. The signal-to-noise ratio of our lidar system can lead to an uncertainty in β_a (z) not exceeding 0.5 %. The $\beta_r(z)$, which is calculated using the temperature and density of air derived from the radiosonde data have an uncertainty within 0.5 % based on Pratt (1985). An uncertainty in the calculation of lidar ratio is within 30 % and the extinction coefficient is estimated with an error of less than 30 % (Chiang et al., 2008a and references therein).

To evaluate the SO_2 measurement errors, the systematic errors from aerosols and other gaseous constituents of the atmosphere, beam misalignment, and statistical

GID
4, 165–190, 2014

errors etc., must be considered. The error analysis can be referred to previous literatures (Schotland, 1974; Vandaele et al., 1994; Fukuchi et al., 1999). In this work, an inaccuracy of less than 30 % were found by comparing the concentration of SO_2 recorded between Continuous Emission Monitoring Systems and DIAL technique.

4 Initial results and discussion

4.1 Determination of overlapping function with a scanning lidar

the overlapping function of lidar defines the efficiency with which the laser beam is coupled with the receiver FOV as a function of height (Povey et al., 2012 and references therein). Accurate estimation of overlapping function describes the accuracy with which lidar can be used to study PBL, where the aerosol distribution is inhomogeneous. In a coaxial lidar system, the backscattered signal at short distances is partly blocked by the secondary mirror of the Schmidt–Cassegrain telescope, and thus indicating that the overlap will depend on the spatial intensity distribution of the beam. Therefore, the horizontal operation of lidar can be used to derive overlap function. The correction is done as: β_{atm} and α (refer Eq. 1) are assumed to be constant for the horizontal atmospheric path. When there is a complete overlapping between transmitter and receiver FOV, the overlap can be canceled and the correction function $O(z)$ becomes 1. By taking the natural logarithm on the both sides of Eq. (1):

$$\ln(P_{\text{M}}(z)\cdot z^2) = \ln(P_{\text{L}}\cdot A_{\text{T}}\cdot \beta_{\text{atm}}) - 2\alpha\cdot z \tag{5}$$

Because the horizontal atmosphere is assumed to be a homogeneous, the term $(P_{\text{L}}\cdot A_{\text{T}}\cdot \beta_{\text{atm}})$ becomes constant. The Eq. (5) describes the expected linear dependence form of the Beer–Lambert relationship, with -2α is slope and $\ln(P_{\text{L}}\cdot A_{\text{T}}\cdot \beta_{\text{atm}})$ is intercepted coefficients. These linear coefficients are determined by fitting a straight-line to $\ln(P_{\text{M}}(z)\cdot z^2)$ over some interval beyond z as shown in Fig. 2. From a linear fit coefficients, the expected signal $\ln(P_{\text{M}}(z)\cdot z^2)$ for a homogeneous path $z < z_0$ (~ 260 m)

GID

4, 165–190, 2014

A new mobile and portable scanning lidar for profiling lower troposphere

C.-W. Chiang et al.

can be calculated. $O(z)$ is then determined by normalizing the measured horizontal signal $S_h(z)$ by expected signal $S_e(z)$,

$$O(z) = S_h(z)/S_e(z). \tag{6}$$

Figure 2b shows the resultant overlap function obtained from the linear fit as shown in Fig. 2a. This result can be used to correct the overlapping functions for scanning lidar observation at short distances. The above technique can be applied to reduce the systematic error in the DIAL system where the overlapping height with telescope FOV is different for two different wavelengths.

4.2 Comparison of extinction coefficient derived from a scanning lidar with particulate matter

The total mass of aerosols per unit volume is termed as a particulate matter (PM). The surface pollution indicated by the $PM_{2.5}/PM_{10}$ (particulate matter with size smaller than 2/10 µm) data are obtained from the Taiwan Environmental Protection Administration (EPA). The EPA monitoring station is about 5 km apart from the lidar site. The $PM_{2.5}/PM_{10}$ data are routinely measured by a Tapered Element Oscillating Microbalance PM monitor (TEOM model 1400a, R&P, Albany, NY, USA). Data is collected consecutively on hourly average for the purpose of legislating, controlling and preventing air pollution.

Figure 3 shows the comparison between the aerosol extinction coefficient derived with lidar at 532 nm and the aerosol mass concentration (in terms of $PM_{2.5}$ and PM_{10}). The extinction coefficient of aerosols derived from the lidar is shown for every 1 min, while $PM_{2.5}/PM_{10}$ is the hourly average data. It is observed that the aerosol extinction coefficient shows good consistency with PM value. The correlation coefficients between the aerosol extinction coefficient and $PM_{2.5}$ concentration, between aerosol extinction coefficient and PM_{10} concentration are respectively 0.73 and 0.85. The better correlation between the aerosol extinction coefficient and PM_{10} concentration may be due

GID
4, 165–190, 2014

A new mobile and portable scanning lidar for profiling lower troposphere

C.-W. Chiang et al.

to the humidity in our location, which plays a crucial role in the growth of hygroscopic aerosols (Chiang et al., 2008b).

4.3 Observation of land-sea breeze using a scanning lidar

The scanning lidar data measured on 26 November 2009 at 02:40 LT (LT = GMT + 08 h) through a vertical scan with a 1° angular resolution is shown in Fig. 4. The data are averaged for every 10 min time interval. The figure shows the 2-D lidar backscattered signal intensity representing cross sections of pollutant concentration in the vertical plane. The scanning profiles clearly characterize the well-defined boundary layer. The depth of the boundary layer is about 500 m, which is consistent with the mean height of PBL (~ 580 m) observed over Chung-Li (Chiang et al., 2008b). The aerosol particles were bounded and rather uniformly mixed within the boundary layer.

To investigate the land-sea breeze, the scanning lidar is directed towards the sea, which is about 6.8 km from the lidar site. Analysis reveals that the study station is affected by the land and sea breezes by observing the movement of aerosol structures. Figure 5 shows the time series contour map of land breeze (top panel) and sea breeze (bottom panel). The results are averaged for every 30 min. During the night, it is observed that the backscattered signal relatively increases as the night progresses (refer Fig. 5 top panel). This could be possibly due to the increase in aerosol concentrations, humidity, descending boundary layer or land breeze onset with the passage of time. When the land breeze increases, the turbulence will also increase. In addition, more humid air will blow from the sea towards the land and will get mixed with aerosol, causing the aerosol hygroscopic growth. The aerosol hygroscopicity factor causes the strong backscattered signal due to their large cross-section area.

In the morning (refer Fig. 5, bottom panel), there is a dense layer near the surface, which is formed by residual layer at night. This layer is lifted up slowly followed with the sunrise and become loose. This phenomenon is referred as convection.

GID
4, 165–190, 2014

4.4 Air Pollution measurement (SO_2)

Figure 6 shows the photograph of the observation site. The inserted box in the figure shows the horizontal observations as a function of range for two different wavelengths used for SO_2 measurement. It can be seen that the differential absorption occurred away from the lidar site, more than 1 km. We refer the different absorption is mainly caused by the human activities since our observing site is located in the outskirts and departed from the bustling city about 2 km. A comparison of SO_2 concentration simultaneously collected on 29 July 2010 between in situ instruments CEMS (Continuous Emission Monitoring Systems) and DIAL measurement is shown in Fig. 7. The lidar is kept fixed at 5° elevation and pointed towards the in situ site. Most of the discrepancies in SO_2 concentration derived from the lidar and CEMS measurements are due to different properties of instruments or dynamics or may be due to ventilation of the atmosphere; however, the both measurements show a similar tendency.

4.5 Application of scanning lidar in monitoring industrial pollutant

Environmental pollution is one of the major concerns in the modern era, especially in the urban and sub-urban areas. Thus, it is of prime importance to monitor the mass concentration of pollutant, their sources and their spatial and temporal variation. The 3-D scanning lidar is very useful in order to characterize the plumes or a fugitive emission from the industrial areas and their sources. This could provide information about the areas which can be affected from these particle concentrations. Figure 8 shows a typical example of backscattered signal intensity measured using scanning lidar over the industrial areas, at Guanyin in Taoyuan County. The pollutant regions are shown on the topographic map (taken from the Google Map) of the industrial areas. The result of a horizontal scan can display 3-D images of the pollutant covering various emitted sources and concentrations within the targeted scan field. This type of scanned figure can be useful in tracking the source and measuring the diffusion range of pollutants within the specified region. This is a useful technique to help the Environmental

GID
4, 165–190, 2014

Protection Administration (EPA) agency to protect people's health and abate the air pollution as quickly as possible.

5 Summary

We have designed and developed a 3-D scanning lidar for the multi-wavelength measurements of aerosol and trace gas, which will be useful in understanding the temporal and spatial variability. The lidar system is designed with small size, light weight, and suitable for installation in various vehicles. It would help to improve the traditional techniques for atmospheric pollutant observations.

The continuous operation of scanning lidar will gather data, which is useful to examine the pollution episode. Such data will also be valuable for understanding the characteristics of pollutant transportation, where the conventional point-sampling instruments have limitation. The scanning lidar gives a new tool to study e.g., formation of the land-sea breeze circulation and variation of PBL by observing the movement of aerosol structures.

The set-up of automatic scanning lidar-network will be helpful in the real-time observation of air pollution over the urban and industrial zones. Such network data will help the EPA to protect the people's health and abate the air pollution as quickly as possible. This could also couple to future policy directives in air pollution abatement strategy.

Acknowledgements. The authors are grateful to the Taiwan EPA for providing the PM data. One of the authors S. K. Das was supported by a Taiwan scholarship during this work and would like to acknowledge the Taiwan Government and National Central University, Chung-Li, Taiwan.

References

Ansmann, A., Bösenberg, J., Chaikovsky, A., Comerón, A., Eckhardt, S., Eixmann, R., Freudenthaler, V., Ginoux, P., Komguem, L., Linné, H., Márquez, M. A. L., Matthias, V., Mattis, I., Mitev, V., Müller, D., Music, S., Nickovic, S., Pelon, J., Sauvage, L., Sobolewsky, P., Srivastava, M.

GID
4, 165–190, 2014
A new mobile and portable scanning lidar for profiling lower troposphere
C.-W. Chiang et al.

Title Page
Abstract | Introduction
Conclusions | References
Tables | Figures
◂ | ▸
Back | Close
Full Screen / Esc
Printer-friendly Version
Interactive Discussion

K., Stohl, A., Torres, O., Vaughan, G., Wandinger, U., and Wiegner, M.: Long-range transport of Saharan dust to northern Europe: the 11–16 October 2001 outbreak observed with EARLINET, J. Geophys. Res., 108, 4783, doi:10.1029/2003JD003757, 2003.

Bach, W.: Global air pollution and climatic change, Rev. Geophys., 14, 429–474, 1976.

Behrendt, A., Wulfmeyer, V., Riede, A.,Wagner, G., Pal, S., Bauer, H., Radlach, M., and Spath, F.: 3-Dimensional observations of atmospheric humidity with a scanning differential absorption lidar, Proceedings of SPIE – the International Society for Optical Engineering, 7475, doi:10.1117/12.835143, 2009.

Behrendt, A., Pal, S., Wulfmeyer, V., Valdebenito, B. A. M., and Lammel, G.: A novel approach for the characterization of transport and optical properties of aerosol particles near sources – Part I: Measurement of particle backscatter coefficient maps with a scanning UV lidar, Atmos. Environ., 45, 2795–2802, 2011.

Browell, E. V., Carter, A. F., Shipley, S. T., Allen, R. J., Butler, C. F., Mayo, M. N., Siviter, Jr., J. H., and Hall, W. M.: NASA multipurpose airborne DIAL system and measurements of ozone and aerosol profiles, Appl. Optics, 22, 522–534, 1983.

Chen, W. N., Tsao, C. C., and Nee, J. B.: Rayleigh lidar temperature measurements in the upper troposphere and lower stratosphere, J. Atmos. Sol.-Terr. Phy., 66, 39–49, 2004.

Chiang, C. W., Chen, W. N., Liang, W. A., and Nee, J. B.: Lidar measurements of spring dusts in 2002 at Chung-Li (25° N, 121° E), Terr. Atmos. Ocean. Sci., 15, 813–824, 2004.

Chiang, C. W., Chen, W. N., Liang, W. A., Das, S. K., and Nee, J. B.: Optical properties of tropospheric aerosols based on measurements of lidar, sunphotometer, and visibility at Chung-Li (25.1° N, 121.1° E), Atmos. Environ., 41, 4128–4137, 2007.

Chiang, C. W., Das, S. K., and Nee, J. B.: An iterative calculation to derive extinction-to-backscatter ratio based on lidar extinction measurement, J. Quant. Spectrosc. Ra., 109, 1187–1195, 2008a.

Chiang, C. W., Das, S. K., and Nee, J. B.: Lidar depolarization measurements for aerosol source and property studies over Chungli (24.58° N, 121.1° E), Atmos. Res., 90, 203–210, 2008b.

Chiang, C. W., Das, S. K., Nee, J. B.„ Hu, S. X., and Hu, H. L.: Simultaneous measurement of humidity and temperature in the lower troposphere over Chung-Li, Taiwan, J. Atmos. Sol.-Terr. Phy., 71, 1389–1396, 2009.

Chiang, C. W., Das, S. K., Lin, C. Y., Nee, J. B., Sun, S. H., Chiang, H. W., Yu, M. J., and Zhang, S. T.: Multi-year investigations of aerosol layer using lidar measurements at Chung-Li, Taiwan, J. Atmos. Sol.-Terr. Phy., 89, 40–47, 2012.

GID

4, 165–190, 2014

Das, S. K., Chiang, C. W., and Nee, J.-B.: Characteristics of cirrus cloud and its radiative properties based on lidar observation Chung-Li, Taiwan, Atmos. Res., 93, 723–735, 2009.
Das, S. K., Chiang, C.-W., and Nee, J. B.: Influence of tropical easterly jet on upper tropical cirrus: an observational study from CALIPSO, Aura-MLS, and NCEP/NCAR data, J. Geophys. Res., 116, D12204, doi:10.1029/2011JD015923, 2011.
Eichinger, W. E., Cooper, D. I., Forman, P. R., Griegos, J., Osborn, M. A., Richter, D., Tellier, L. L., and R. Thornton, R.: The development of a scanning Raman water vapor lidar for boundary layer and tropospheric observations, J. Atmos. Ocean. Tech., 16, 1753–1766, 1999.
Eilts, M., Doviak, R., and Sundara-Rajan, A.: Comparison of winds, waves, and turbulence as observed by airborne lidar, ground-based radars, and instrumented tower, Radio Sci., 19, 1511–1522, 1984.
Ferdinando, D. T., Parrone, M. R., and Protopapa, M. L.: Monitoring O_3 with solar-blind Raman Lidars, Appl. Optics, 40, 1314–1320, 2001.
Fredriksson, K., Galle, B., Nystrom, K., and Svanberg, S.: Mobile LIDAR system for environmental probing, Appl. Optics, 20, 4181–4189, 1981.
Fukuchi, T., Goto, N., Fujii, T., and Nemoto, K.: Error analysis of SO_2 measurement by multiwavelength differential absorption lidar, Opt. Eng., 38, 141–145, doi:10.1117/1.602068, 1999.
Gimmestad, G. G.: Differential-absorption lidar for ozone and industrial emissions, in: Lidar – Range-Resolved Optical Remote Sensing of the Atmosphere, edited by: Weitkamp, C., Springer, New York, 187–212, 2005.
Kaufman, Y. J., Tanre, D., and Boucher, O.: A satellite view of aerosols in the climate system, Nature, 419, 215–224, 2002.
Li, T., Leblanc, T., and McDermid, I. S.: Interannual variations of middle atmospheric temperature as measured by the JPL lidar at Mauna Loa Observatory, Hawaii (19.5° N, 155.6° W), J. Geophys. Res., 113, D14109, doi:10.1029/2007JD009764, 2008.
Mattis, I., Ansmann, A., Müller, D., Wandinger, U., and Althausen, D.: Multiyear aerosol observations with dual-wavelength Raman lidar in the framework of EARLINET, J. Geophys. Res., 109, D13203, doi:10.1029/2004JD004600, 2004.
Mayor, S. and Spuler, S.: Raman-shifted eye-safe aerosol lidar, Appl. Optics, 43, 3915–3924, 2004.

GID
4, 165–190, 2014

McGill, M. J., Hlavka, D. L., Hart, W. D., Spinhirne, J. D., Scott, V. S., and Schmid, B.: The Cloud Physics Lidar: instrument description and initial measurement results, Appl. Optics, 41, 3725–3734, 2002.
Megie, G. and Menzies, R. T.: Complementarity of UV and IR differential absorption lidar for global measurements atmospheric species, Appl. Optics, 1173–1183, 1980.
Murayama, T., Sugimoto, N., Uno, I., Kinoshita, K., Aoki, K., Hagiwara, N., Liu, Z., Matsui, I., Sakai, T., Shibata, T., Arao, K., Sohn, B. J., Won, J. G., Yoon, S. C., Li, T., Zhou, J., Hu, H., Abo, M., Iokibe, K.,Koga, R., and Iwasaka, Y.,: Ground-based network observation of Asian dust events of April 1998 in east Asia, J. Geophys. Res., 106, 18345–18359, doi:10.1029/2000JD900554, 2001.
Nee, J., Wang, G., Lee, P., and Lin, S.: Lidar studies of particles and temperatures of the atmosphere: first results from National Central University lidar, Radio Sci., 30, 1167–1175, 1995.
Papayannis, A., Ancellet, G., Pelon, J., and Megie, G.: Multiwavelength lidar for ozone measurements in the troposphere and the lower stratosphere, Appl. Optics, 29, 467–476, 1990.
Pratt, R. W.: Review of radiosonde humidity and temperature errors, J. Atmos. Ocean. Tech., 2, 404–407, 1985.
Povey, A. C., Grainger, R. G., Peters, D. M., Agnew, J. L., and Rees, D.: Estimation of a lidar's overlap function and its calibration by nonlinear regression, Appl. Optics, 51, 5130–5143, 2012.
Radlach, M., Behrendt, A., and Wulfmeyer, V.: Scanning rotational Raman lidar at 355 nm for the measurement of tropospheric temperature fields, Atmos. Chem. Phys., 8, 159–169, doi:10.5194/acp-8-159-2008, 2008.
Sasano, Y.: Observational study on the atmospheric mixed layer and transition layer structures using a Mie lidar, J. Meteorol. Soc. Jpn., 63, 419–435, 1985.
Schotland, R. M.: Errors in the lidar measurement of atmospheric gases by differential absorption, J. Appl. Meteorol., 13, 71–77, 1974.
Sivakumar, V., Bhavanikumar, Y., Rao, P. B., Mizutani, K., Aoki, T.,Yasui, T., and Itabe, T.: Lidar observed characteristics of the tropical cirrus clouds, Radio Sci., 38, 1094, doi:10.1029/2002RS002719, 2003.
Staehr, W., Lahmann, W., and Weitkamp, C.: Range-resolved differential absorption lidar: optimization of range and sensitivity, Appl. Optics, 24, 1950–1956, 1995.
Twomey, S. A.: Aerosols, clouds and radiation, Atmos. Environ., 25, 2435–2442, 1991.

Vandaele, A. C., Simon, P. C., Guilmot, J. M., Carleer, M., and Colin, R.: SO_2 absorption cross section measurement in the UV using a Fourier transform spectrometer, J. Geophys. Res., 99, 25599–25605, 1994.

Wandinger, U.: Introduction to lidar, in: Lidar – Range-Resolved Optical Remote Sensing of the Atmosphere, edited by: Weitkamp, C., Springer, New York, 1–18, 2005.

Wulfmeyer, V. and Bösenberg, J.: Ground-based differential absorption lidar for water-vapor profiling: assessment of accuracy, resolution, and meteorological applications, Appl. Optics, 37, 3825–3844, 1998.

GID

4, 165–190, 2014

A new mobile and portable scanning lidar for profiling lower troposphere

C.-W. Chiang et al.

Table 1. Technical specifications of scanning lidar.

Transmitter	
Laser	Nd:YAG Laser
Wavelength (nm)	266/355/532 nm
Pulse energy (mJ)	95/160/387 mJ
Repetition rate (Hz)	20 Hz
Beam divergence	0.5 mrad
Pulse duration	10 ns
Raman Cell length	1.5 m
Raman Output wavelength	
H_2 (5 atm) at 266 nm	298 nm
CH_4 (20 atm) at 266/355 nm	289/395 nm
Reciever	
Telescope type	Schmidt–Cassegrain (Diameter 20 cm)
Detector	Head-on PMT, Hamamatsu R7400
Filters	0.2–3 nm FWHM
Scanner	
Scan type	Azimuth-elevation
Scan rate	600–0.25 deg/min
Signal processor	
Type	Digital processing
Sample rate	250 MHz

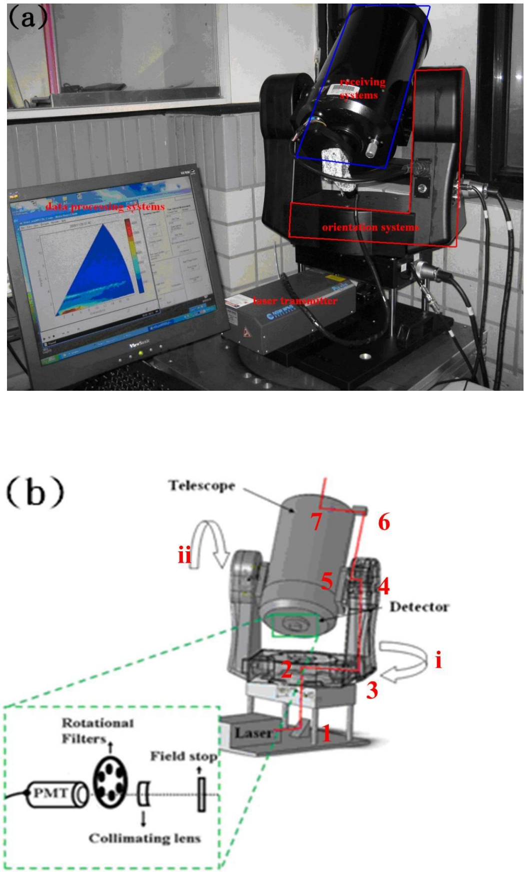

Fig. 1. (a) Pictorial image and **(b)** prototype model of the 3-D scanning lidar system. In figure **(b)**, the arrows i and ii show the zenith and azimuth scanning direction. Red line shows the path of the transmitting laser beam. The numbers 1 to 6 shows the position of reflection mirror. The receiver section is shown in the enlarged box in green.

GID
4, 165–190, 2014

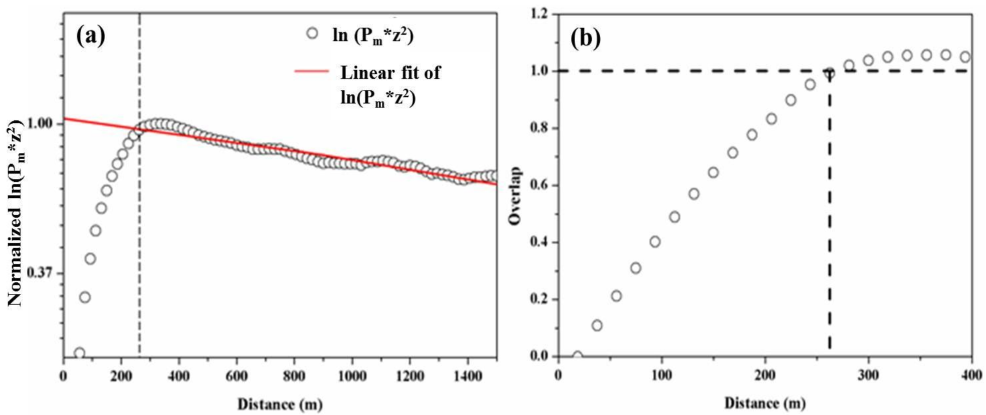

Fig. 2. Overlap function determination by keeping scanning lidar fixed in horizontal direction. Figure **(a)** shows a linear fit ($y = -2.43 \cdot 10^{-4} \cdot x + 1.03$, shown as a solid red line) applied to the horizontal data ln(Pm*z2) to determine the expected signal response for the range below overlap height (~ 260 m). Figure **(b)** shows the resultant overlap function obtained from horizontal data ln(Pm*z2) divided by expected signal.

GID
4, 165–190, 2014

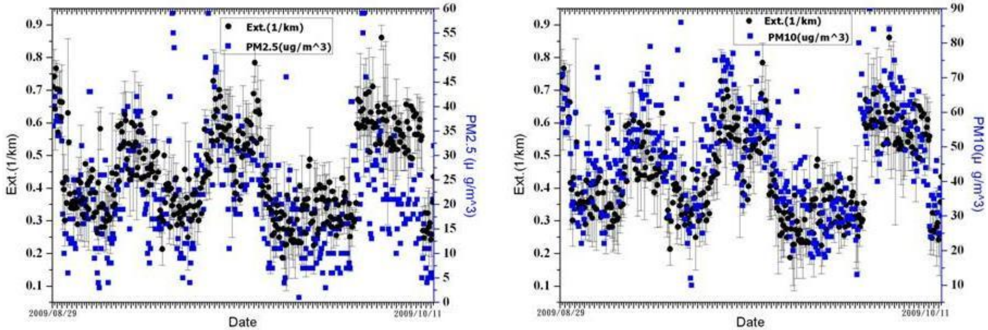

Fig. 3. Comparison of **(a)** $PM_{2.5}$ and **(b)** PM_{10} concentration with the aerosol extinction coefficient derived from the scanning lidar. The PM data are hourly average; while the lidar data are shown for every 1 min. Error bars indicate the standard deviation of aerosol extinction coefficient.

GID
4, 165–190, 2014

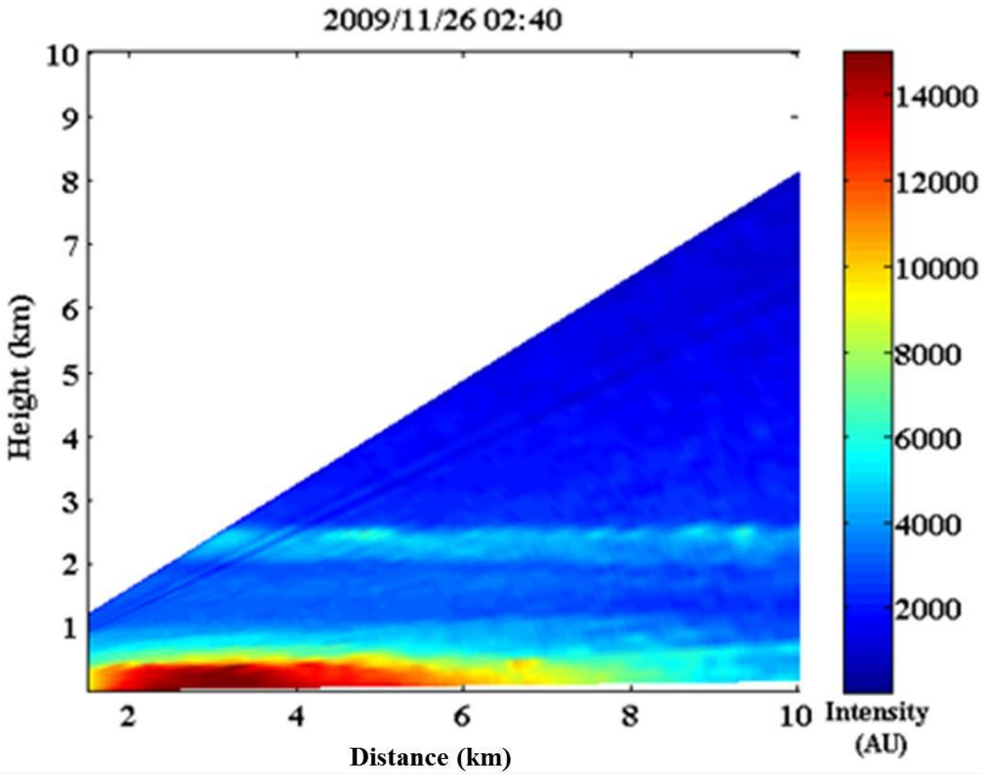

Fig. 4. Lidar range height indicator (RHI) scans of lower troposphere on 26 November 2009.

GID
4, 165–190, 2014

A new mobile and portable scanning lidar for profiling lower troposphere

C.-W. Chiang et al.

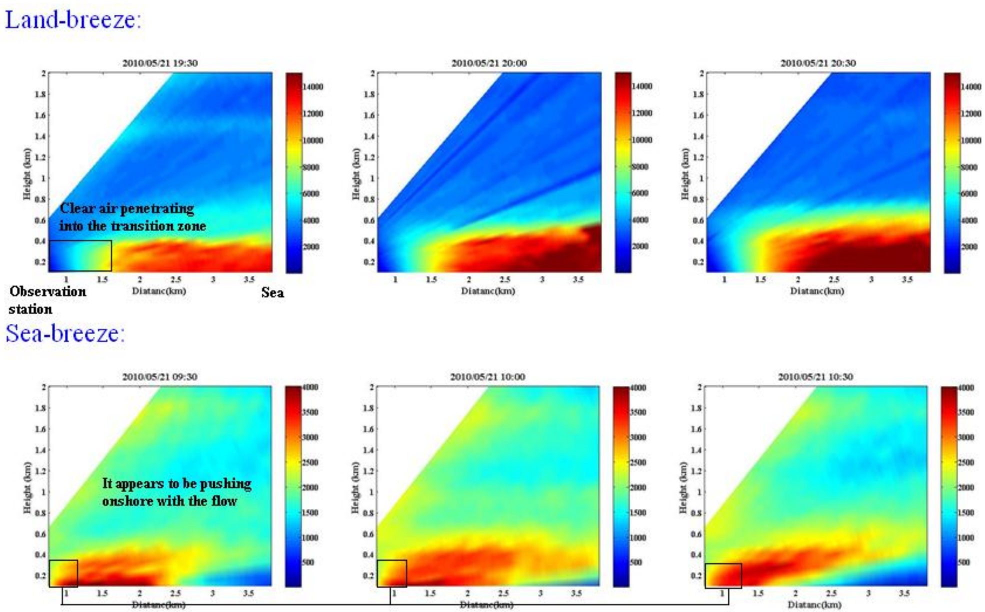

Fig. 5. Lidar vertical cross-section of land (top) and sea (bottom) breeze cases.

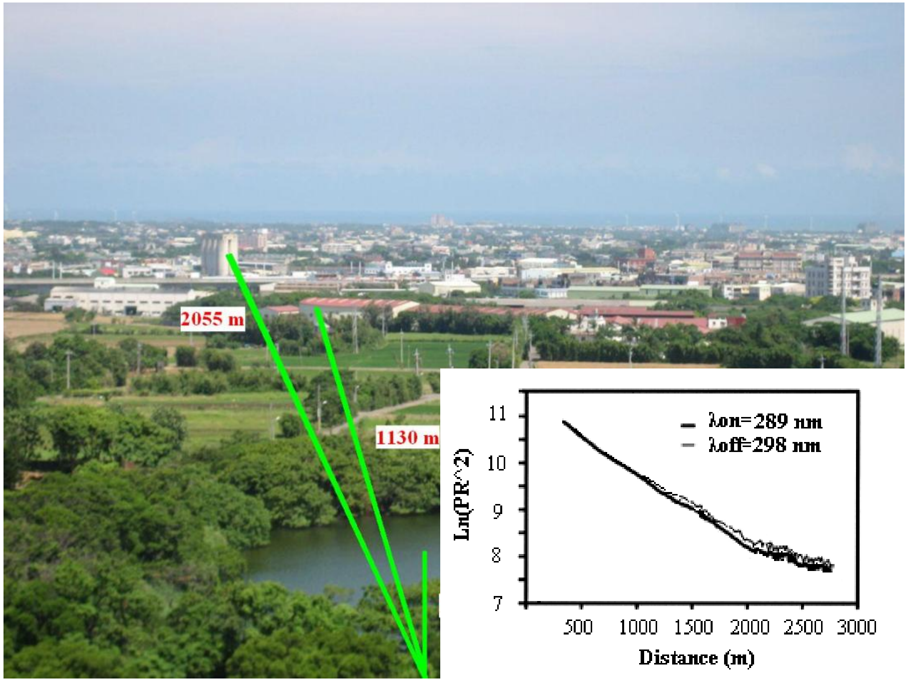

Fig. 6. DIAL measurement of SO_2 at observation station on 7 June 2010.

GID
4, 165–190, 2014

A new mobile and portable scanning lidar for profiling lower troposphere

C.-W. Chiang et al.

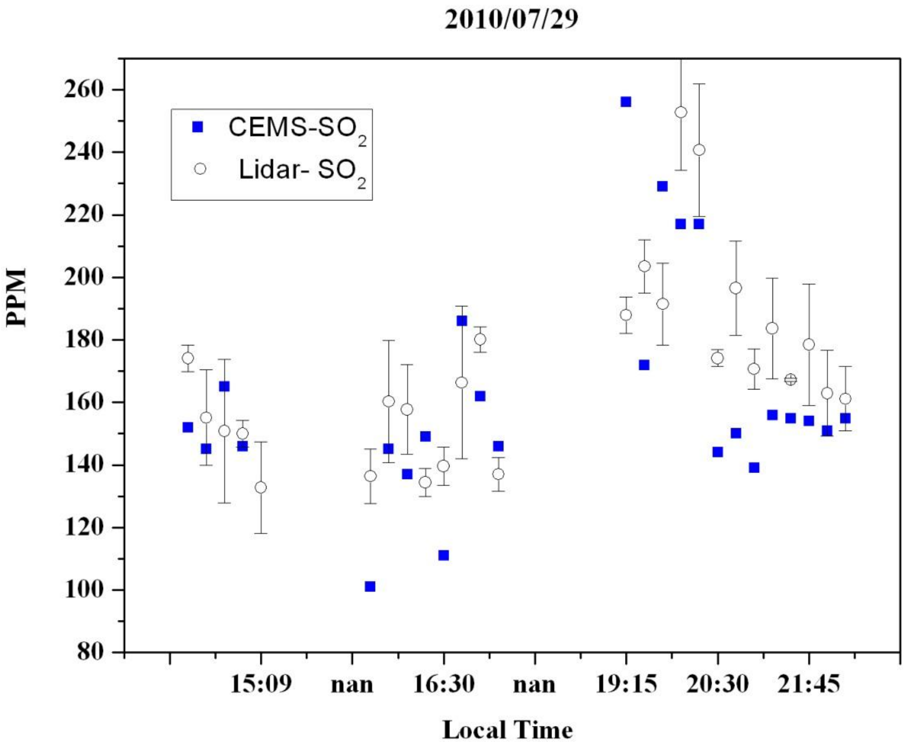

Fig. 7. Comparison of SO_2 concentration simultaneously measured from the DIAL and in-situ instruments (CEMS) on 29 July 2010. Error bars indicate the statistical SO_2 concentration uncertainty derived from the DIAL measurement.

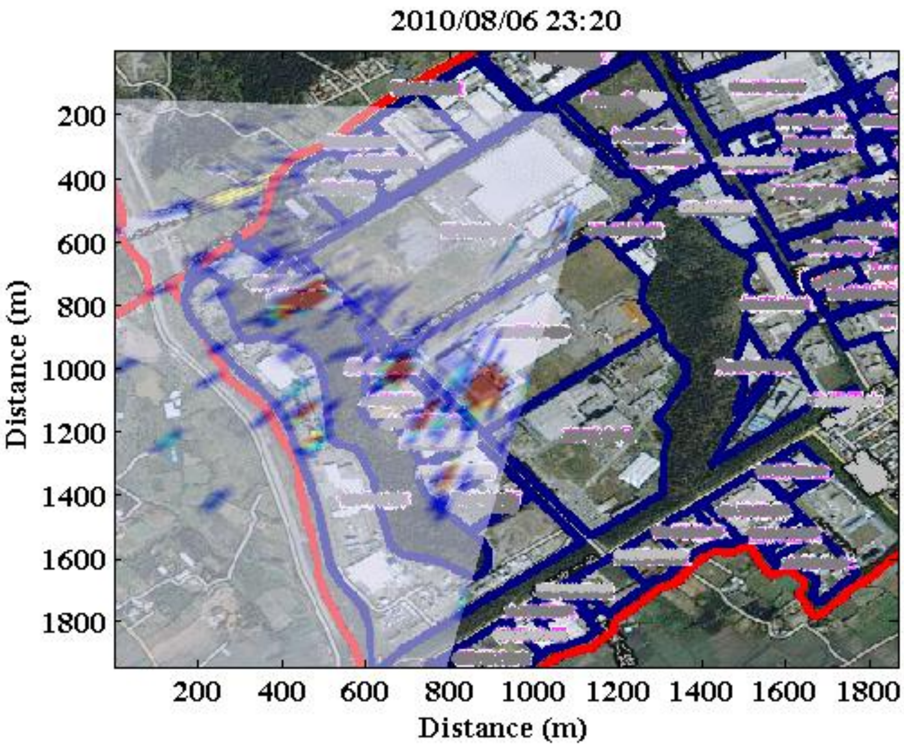

Fig. 8. A sector scan of lidar overlapped on the topographical map (courtesy: Google Map).